Full-Wave Analysis of Lossy Quasi-Planar Transmission Line Incorporating the Metal Modes

CHING-KUANG C. TZUANG, MEMBER, IEEE, CHU-DONG CHEN, STUDENT MEMBER, IEEE, AND SONG-TSUEN PENG, FELLOW, IEEE

Abstract—**We present a novel and accurate full-wave mode-matching approach to analyze the dispersion characteristics of millimeter-wave and microwave transmission lines with finite conductivity, metallization thickness, and holding grooves. The approach is quite general but only the results for a unilateral finline are presented. The accuracy of the solution depends primarily on the correct and complete description of eigenfunction expansions in each of the uniform (stratified) or nonuniform layer regions. The latter consists of metallized strips of finite conductivity, which in turn produce the so-called metal modes (eigenmodes). The metal mode exists in the metallized region with high conductivity for the most part and decays sharply in the air region. Without incorporating the metal modes, the convergence studies will fail and the accuracy of the field theory solution deteriorates.**

Since the accuracy of the present approach is established, the composite effects of the finite conductivity and metallization thickness can be studied rigorously. A numerical limiting case analysis shows that the mode conversion between the dominant finline mode and the dielectric-slab-loaded waveguide mode may happen through the reduction of the metallization thickness. The theoretical results for the dispersion parameters of the dominant mode propagation constant and the characteristic impedance are reported. The effects of the conductor losses using various metallizing materials are also presented.

I. INTRODUCTION

THE ANALYSIS of conductor losses on integrated millimeter-wave and microwave transmission lines plays an important role in the accurate computer-aided design (CAD) modeling required in many demanding applications. Three mechanisms constitute the attenuation in the transmission lines, namely, conductor loss, dielectric loss, and radiation loss [1]. The effects of dielectric losses on transmission lines have been analyzed thoroughly [2], [3]. This paper will focus on the propagation characteristics of an electrically shielded transmission line for use in millimeter-wave and microwave component design. Therefore, we will restrict our attention to conductor loss. Recently, a few methods have been developed for this, among them a combined surface integral equation method [4], a phenomenological loss equivalence method [5], and a modified mode-matching method [6].

In formulating the combined surface integral equation [4], prior knowledge of quasi-TEM analysis of the field penetration into the microstrip line is required for later formulation. The phenomenological loss equivalence method is developed for a transmission line which supports a quasi-TEM mode with conductor thickness of the order of the skin depth. For an integrated finline, however, the above methods need modifications because the dominant mode is not quasi-TEM. In certain applications when a low-impedance microstrip line needs to operate at very high frequency, the quasi-TEM assumption fails to model the microstrip line faithfully.

By way of example, Fig. 1 shows an electrically shielded symmetrical lossless microstrip line integrated on a 100-μm-thick GaAs substrate ($\epsilon_r = 13$) that is analyzed by the spectral-domain approach (SDA) using a highly effective set of basis functions [7]. When operating at 150 GHz, the results indicate that the longitudinal and transverse surface current densities, J_z and J_x, are comparable in magnitude for impedances lower than 17.0 Ω. For the 32.4 Ω microstrip line, the transverse current component is about 1/15 the longitudinal component. Thus, depending on the structure and operating frequency, the quasi-TEM assumption may not apply for millimeter-wave circuit designs. Another full-wave approach for analyzing a transmission line with conductor losses is the perturbational method [8], [9]. This approach assumes that the quasi-planar transmission lines have infinitely thin metallization with conductivity of infinite value. After the lossless full-wave solution is obtained, a perturbational expression is invoked for computing the conductor loss, e.g. [8, eq. (11)]. The assumption is apparently valid for structures with small losses.

It is difficult, however, to track the tangled effects of the finite conductivity, finite metallization thickness, and broad operating frequencies covered in the millimeter-wave and microwave regimes without skillfully managing the above-mentioned assumptions or simplifications. This paper presents a reliable and accurate method for solving the above problems by the full-wave mode-matching

Manuscript received March 29, 1990; revised August 20, 1990. This work was supported in part by the Taiwan National Science Council under Grant NSC79-0404-E009-29 and Contract D78026.

C.-K. C. Tzuang and C.-D. Chen are with the Institute of Communication Engineering and the Center for Telecommunication Research, National Chiao Tung University, No. 75, Po Ai Street, Hsinchu, Taiwan, Republic of China.

S.-T. Peng is with the Electrical Engineering Department, New York Institute of Technology, Old Westbury, NY 11568.

IEEE Log Number 9040054.

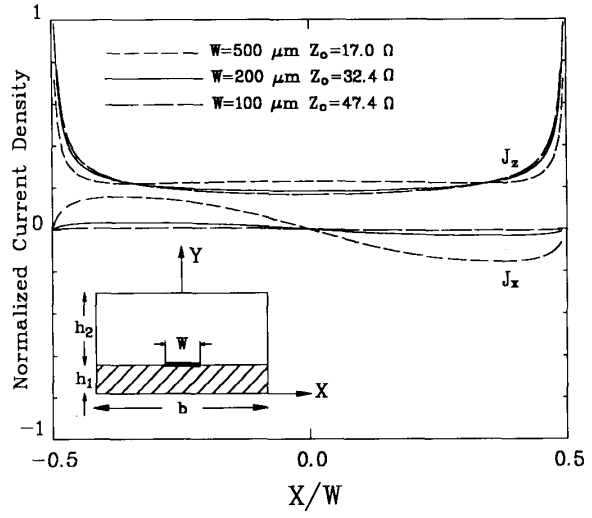

Fig. 1. Longitudinal (J_z) and transverse (J_x) surface current densities of a lossless microstrip line integrated on a GaAs substrate at 150 GHz. $b = 10$ mm, $h_1 = 100$ μm, and $h_2 = 1$ mm.

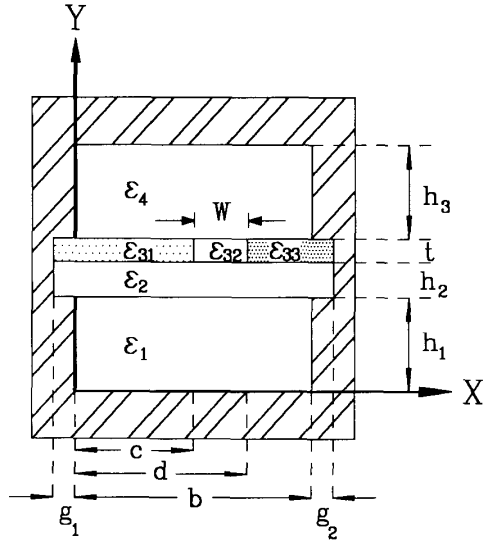

Fig. 2. A unilateral finline with finite conductivity, metallization thickness, and holding grooves. $b = 3.556$ mm, $c = 1.6002$ mm, $d = 1.9558$ mm, $g_1 = g_2 = 0$, $h_1 = 3.4925$ mm, $h_2 = 0.127$ mm, $t + h_3 = 3.4925$ mm, $\epsilon_1 = \epsilon_{32} = \epsilon_4 = 1$, $\epsilon_2 = 2.22$, $\epsilon_{31} = \epsilon_{33} = 1 - j\sigma/\omega\epsilon_0$, and $\sigma = 3.333 \times 10^7$ mhos/m.

method [6], [10], [11]. The solutions are correct in the sense that the numerically truncated solutions should satisfy the so-called relative and absolute convergence criteria [10]–[13] for various lossless waveguide structures. The convergence study is further complicated by the inclusion of the metal modes in the mode-matching formulation [14]. In this paper a series of convergence studies is presented for a unilateral finline to illustrate the convergence properties of the present formulation taking into account the conductor losses. Such an accurate field theory approach enables us to investigate important propagation characteristics of transmission lines involving finite metallization thicknesses and conductivities.

II. Formulation: A Mode-Matching Method Incorporating the Metal Modes

Fig. 2 illustrates a particular example to be analyzed rigorously. The quasi-planar transmission line is surrounded by a perfectly conducting enclosure. The waveguide cross section is subdivided into six regions with their respective relative dielectric constants. The subscript of each relative dielectric constant is the name of that region. Thus, region 31 is the region with relative dielectric constant ϵ_{31}. Throughout this paper, the $e^{j\omega t - \gamma z}$ factor is assumed. Therefore, for a lossy transmission line, we will expect a complex propagation constant γ ($\gamma = \alpha + j\beta$) to exist. For a metallized region of finite conductivity, $\epsilon_{3r} = \epsilon_r - j\sigma/\omega\epsilon_0$, where σ is the conductivity of the metallization. If regions 1 and 4 are air-filled and region 2 is the supporting dielectric substrate, Fig. 2 may become two different quasi-planar transmission lines. When regions 31 and 33 are metallized and region 32 is air-filled, the structure is a unilateral finline. The reverse of this is a suspended microstrip line. This paper will focus on the analysis of the unilateral finline to study the important physical characteristics of the lossy finline without loss of generality.

The mode-matching formulation based on the TM-to-x and TE-to-x eigenfunction expansions for all regions is derived. They are summarized as follows.

Region 1:

$$\Psi_1^e = \sum_{n=0}^{N_1} A_n^e \cos[\alpha_{1n}x] \frac{\sin[\beta_{1n}y]}{\sin[\beta_{1n}h_1]} \tag{1}$$

$$\Psi_1^h = \sum_{n=1}^{N_1} B_n^h \sin[\alpha_{1n}x] \frac{\cos[\beta_{1n}y]}{\cos[\beta_{1n}h_1]} \tag{2}$$

$$(\alpha_{1n} = n\pi/b).$$

Region 2:

$$\Psi_2^e = \sum_{n=0}^{N_2} \cos[\alpha_{2n}(x + g_1)] \cdot \left\{ C_n^e \frac{\cos[\beta_{2n}(y - h_1)]}{\cos[\beta_{2n}h_2]} + D_n^e \frac{\sin[\beta_{2n}(y - h_1)]}{\sin[\beta_{2n}h_2]} \right\} \tag{3}$$

$$\Psi_2^h = \sum_{n=1}^{N_2} \sin[\alpha_{2n}(x + g_1)] \cdot \left\{ C_n^h \frac{\cos[\beta_{2n}(y - h_1)]}{\cos[\beta_{2n}h_2]} + D_n^h \frac{\sin[\beta_{2n}(y - h_1)]}{\sin[\beta_{2n}h_2]} \right\} \tag{4}$$

$$(\alpha_{2n} = n\pi/(g_1 + b + g_2)).$$

Region 3:

$$\Psi_3^e = \sum_{n=0}^{N_3} \Phi_{3n}^e(x)\left\{E_n^e \frac{\cos\left[\beta_{3n}^e(h_1+h_2+t-y)\right]}{\cos\left[\beta_{3n}^e t\right]} + F_n^e \frac{\sin\left[\beta_{3n}^e(h_1+h_2+t-y)\right]}{\sin\left[\beta_{3n}^e t\right]}\right\} \quad (5)$$

$$\Psi_3^h = \sum_{n=1}^{N_3} \Phi_{3n}^h(x)\left\{E_n^h \frac{\cos\left[\beta_{3n}^h(h_1+h_2+t-y)\right]}{\cos\left[\beta_{3n}^h t\right]} + F_n^h \frac{\sin\left[\beta_{3n}^h(h_1+h_2+t-y)\right]}{\sin\left[\beta_{3n}^h t\right]}\right\} \quad (6) \quad (6)$$

$$N_3 = N_{31} + N_{32} + N_{33}$$

where N_{31}, N_{32}, and N_{33} can be either the number of metal modes or the number of air modes. When analyzing Fig. 2 as a unilateral finline, N_{31} and N_{33} are the numbers of metal modes associated with the metallized fins, whereas N_{32} is the number of air modes corresponding to the gap:

Region 4:

$$\Psi_4^e = \sum_{n=0}^{N_4} G_n^e \cos\left[\alpha_{4n}x\right] \frac{\sin\left[\beta_{4n}(h_1+h_2+t+h_3-y)\right]}{\sin\left[\beta_{4n}h_3\right]} \quad (10)$$

$$\Psi_4^h = \sum_{n=1}^{N_4} H_n^h \sin\left[\alpha_{4n}x\right] \frac{\cos\left[\beta_{4n}(h_1+h_2+t+h_3-y)\right]}{\cos\left[\beta_{4n}h_3\right]} \quad (11)$$

$$(\alpha_{4n} = n\pi/b).$$

Because the sidewalls of the waveguide housing are assumed to be perfect electric conductors, the biorthogonality relationship holds for eigenfunctions in region 3, although it contains a lossy conductor layer [15]. The biorthogonality relationship in this region reads as

$$\int_{-g_1}^{b+g_2} \Phi_{3m}^h(x)\Phi_{3n}^h(x)\,dx = \delta_m^n \quad (12)$$

$$\int_{-g_1}^{b+g_2} \Phi_{3m}^e(x)\frac{\Phi_{3n}^e(x)}{\epsilon_{3r}(x)}\,dx = \delta_m^n \quad (13)$$

where δ_m^n is the Kronecker delta function.

$$\Phi_{3n}^e(x) = \begin{cases} \alpha_n^e \dfrac{\cos\left[\alpha_{31n}^e(x+g_1)\right]}{\cos\left[\alpha_{31n}^e(g_1+c)\right]}, & x \in [-g_1, c] \\ \kappa_n^e \dfrac{\cos\left[\alpha_{32n}^e(x-(c+d)/2)\right]}{\cos\left[\alpha_{32n}^e W/2\right]} + \beta_n^e \dfrac{\sin\left[\alpha_{32n}^e(x-(c+d)/2)\right]}{\cos\left[\alpha_{32n}^e W/2\right]}, & x \in [c, d] \\ \gamma_n^e \dfrac{\cos\left[\alpha_{33n}^e(b+g_2-x)\right]}{\cos\left[\alpha_{33n}^e(b-d+g_2)\right]}, & x \in [d, b+g_2] \end{cases} \quad (7)$$

$$\Phi_{3n}^h(x) = \begin{cases} \alpha_n^h \dfrac{\sin\left[\alpha_{31n}^h(x+g_1)\right]}{\sin\left[\alpha_{31n}^h(g_1+c)\right]}, & x \in [-g_1, c] \\ \kappa_n^h \dfrac{\cos\left[\alpha_{32n}^h(x-(c+d)/2)\right]}{\cos\left[\alpha_{32n}^h W/2\right]} + \beta_n^h \dfrac{\sin\left[\alpha_{32n}^h(x-(c+d)/2)\right]}{\cos\left[\alpha_{32n}^h W/2\right]}, & x \in [c, d] \\ \gamma_n^h \dfrac{\sin\left[\alpha_{33n}^h(b+g_2-x)\right]}{\sin\left[\alpha_{33n}^h(b-d+g_2)\right]}, & x \in [d, b+g_2] \end{cases} \quad (8)$$

where

$$\left(\alpha_{31n}^i\right)^2 = \epsilon_{31}\beta_0^2 - \left(\beta_{3n}^i\right)^2 + \gamma^2$$

$$\left(\alpha_{32n}^i\right)^2 = \epsilon_{32}\beta_0^2 - \left(\beta_{3n}^i\right)^2 + \gamma^2$$

$$\left(\alpha_{33n}^i\right)^2 = \epsilon_{33}\beta_0^2 - \left(\beta_{3n}^i\right)^2 + \gamma^2$$

$$\beta_0^2 = \omega^2\mu_0\epsilon_0, \qquad i = e \text{ or } h. \quad (9)$$

The values of $\alpha_n^{e,h}$, $\kappa_n^{e,h}$, $\beta_n^{e,h}$, $\gamma_n^{e,h}$, $\alpha_{31n}^{e,h}$, $\alpha_{32n}^{e,h}$, and $\alpha_{33n}^{e,h}$ can be obtained in the same way as in a dielectric-slab-loaded waveguide problem and will not be repeated here [15].

The above equations indicate that 12 sets of unknown coefficients exist. These coefficients can be eliminated by matching all the necessary tangential boundary conditions at each interface and applying the biorthogonality relationship governed by (12) and (13). Finally a nonstandard eigenvalue equation is derived, i.e.,

$$[\boldsymbol{A}(\gamma)][\boldsymbol{x}] = [\boldsymbol{0}] \quad (14)$$

where the column vector is $[\boldsymbol{x}] = [\boldsymbol{C}_n^h\ \boldsymbol{D}_n^e\ \boldsymbol{E}_n^h\ \boldsymbol{F}_n^e]^T$, which contains the remainder sets of coefficients. The matrix $[\boldsymbol{A}]$ has the size $2(N_2+N_3+1)$ by $2(N_2+N_3+1)$. The roots of the equation $\det([\boldsymbol{A}(\gamma)]) = 0$ give rise to the solutions for the complex propagation constants. The nontrivial solution directly leads to the solution for $[\boldsymbol{x}]$.

TABLE I
EIGENVALUES OF METAL AND AIR MODES IN REGION 3 (FIG. 2) AT A FREQUENCY OF 40 GHz

		TM mode			TE mode		
		α^{e}_{31n}/β_o	α^{e}_{32n}/β_o	α^{e}_{33n}/β_o	α^{h}_{31n}/β_o	α^{h}_{32n}/β_o	α^{h}_{33n}/β_o
AIR MODE	$N_{32}=0$	$2.73\times10^{3}-j2.73\times10^{3}$	$1.59\times10^{-2}+j3.84\times10^{-2}$	$2.73\times10^{3}-j2.73\times10^{3}$			
	$N_{32}=1$	$2.73\times10^{3}-j2.73\times10^{3}$	$1.05\times10^{1}+j1.16\times10^{-4}$	$2.73\times10^{3}-j2.73\times10^{3}$	$2.73\times10^{3}-j2.73\times10^{3}$	$1.05\times10^{1}+j1.28\times10^{-2}$	$2.73\times10^{3}-j2.73\times10^{3}$
	$N_{32}=2$	$2.73\times10^{3}-j2.73\times10^{3}$	$2.10\times10^{1}+j5.81\times10^{-5}$	$2.73\times10^{3}-j2.73\times10^{3}$	$2.73\times10^{3}-j2.73\times10^{3}$	$2.10\times10^{1}+j2.57\times10^{-2}$	$2.73\times10^{3}-j2.73\times10^{3}$
METAL MODE	$N_{31}=1$	$1.17\times10^{0}-j1.06\times10^{-11}$	$2.73\times10^{3}+j2.73\times10^{3}$	$1.17\times10^{0}-j1.92\times10^{-4}$	$2.34\times10^{0}-j3.19\times10^{-4}$	$2.73\times10^{3}+j2.73\times10^{3}$	$2.34\times10^{0}-j4.15\times10^{-4}$
	$N_{31}=2$	$3.51\times10^{0}-j3.19\times10^{-11}$	$2.73\times10^{3}+j2.73\times10^{3}$	$3.51\times10^{0}-j6.40\times10^{-4}$	$4.68\times10^{0}-j6.38\times10^{-4}$	$2.73\times10^{3}+j2.73\times10^{3}$	$4.68\times10^{0}-j6.86\times10^{-4}$
	$N_{31}=3$	$5.85\times10^{0}-j5.32\times10^{-11}$	$2.73\times10^{3}+j2.73\times10^{3}$	$5.85\times10^{0}-j3.84\times10^{-4}$	$7.02\times10^{0}-j9.57\times10^{-4}$	$2.73\times10^{3}+j2.73\times10^{3}$	$7.02\times10^{0}-j9.89\times10^{-4}$

Given the solution for $[x]$, the characteristic impedance can be obtained in the same way as in [12].

III. METAL MODES AND AIR MODES

Section II presents a classical mode-matching method which is distinguished from the conventional one by the inclusion of the metal modes. Regions 1, 2, and 4 are expanded in a way similar to that in [12]. The eigenfunctions in these regions are classified as air modes. For a lossy unilateral finline, regions 31, 32, and 33 should have both air modes and metal modes to provide the mode completeness required in the mode-matching method. The first few TM-to-x air modes in the air region 32 and TM-to-x metal modes in the lossy conductor region 31 were reported in [14, figs. 2 and 3] and will not be repeated here. To further clarify the concept of using both air modes and metal modes, Table I lists the values of the first three eigenvalues at 40 GHz for air modes of region 32 and metal modes of region 31 for the structural parameters shown in Fig. 2. When the conductivity is high, the eigenfunction corresponding to the metal mode confines itself in the metal region and decays abruptly in the air region. The eigenfunction corresponding to the air mode is much more familiar to us. In contrast to the metal mode, the air mode resides mostly in the air (dielectric) region bounded by good metals.

IV. CONVERGENCE STUDIES FOR A PARTICULAR LOSSY FINLINE

As pointed out by various authors interested in analyzing the propagation characteristics of lossless waveguide structures using the mode-matching method, the relative convergence criterion should be satisfied to obtain good field matchings at discontinuities or interfaces [10]–[13]. Failing to do this will result in inaccurate field solutions. In the case of a lossy quasi-planar transmission line, the convergence study is further complicated by the existence of the metal modes described in Section III. Since most millimeter-wave and microwave integrated transmission lines are gold-plated to reduce the conductor losses that inevitably exist in these structures, we restrict our attention to the convergence study for a transmission line with a good conductor coating. Under this condition and using the structural and material parameters listed in Fig. 2, Figs. 3 to 5 summarize the results for the convergence study.

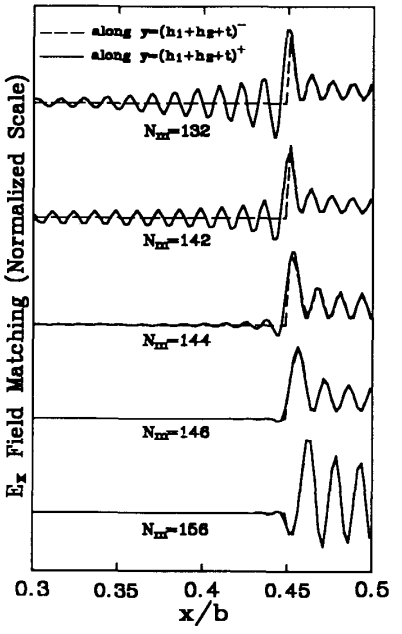

Fig. 3. Relative convergence studies of the tangential electric field E_x at the interfaces $y=(h_1+h_2+t)^-$ and $y=(h_1+h_2+t)^+$ for various numbers of metal modes N_m ($N_m=N_{31}+N_{33}$) at 40 GHz. $N_1=N_2=N_4=160$, $N_a=N_{32}=16$, $t=5$ μm, and $W/b=0.1$. (Other structural and material parameters are listed in Fig. 2.)

The number of expansion terms used in the formulation in regions 1 to 4 are N_1, N_2, N_{31}, N_{32}, N_{33}, and N_4, respectively. In the particular case study for a symmetrical lossy finline, the sum of N_{31} and N_{33} is renamed N_m, which represents the number of metal modes. N_{32} is renamed N_a, i.e., the number of air modes. When analyzing the complex modes of a lossless bilateral finline, it was found that the relative convergence criterion should be simultaneously satisfied at the interfaces near the dual slots to obtain the best field matchings in the interfaces [12]. Since the symmetrical unilateral finline under investigation assumes 5-μm-thick gold-plated strips and the

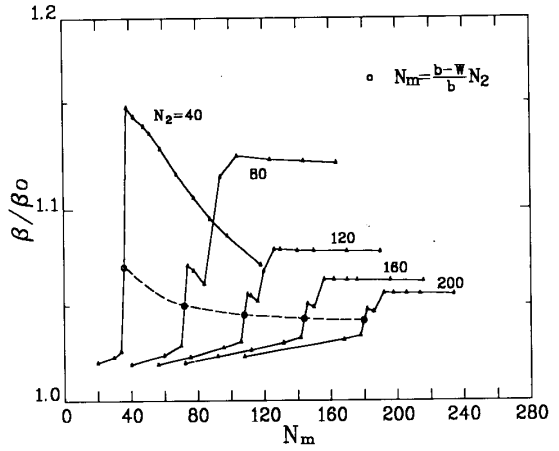

Fig. 4. Relative and absolute convergence studies of the normalized propagation constant for the dominant mode versus the value of N_m under different controlling parameter:

$N_1 = N_2 = N_4 = 40$ $N_a = 4$
$N_1 = N_2 = N_4 = 80$ $N_a = 8$
$N_1 = N_2 = N_4 = 120$ $N_a = 12$
$N_1 = N_2 = N_4 = 160$ $N_a = 16$
$N_1 = N_2 = N_4 = 200$ $N_a = 20$.

$W/b = 0.1$, $t = 5$ μm, and frequency = 40 GHz. (Other structural and material parameters are listed in Fig. 2.)

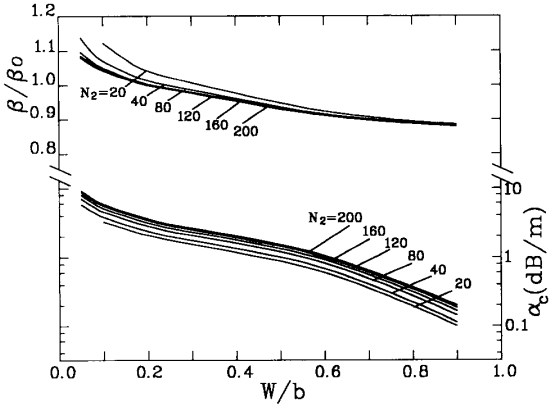

Fig. 5. Absolute convergence studies of the complex propagation constant for the dominant mode versus the normalized fin gap W/b; $t = 5$ μm and frequency = 40 GHz. The N_m values are determined by the aspect ratio discussed in Figs. 3 and 4. (Other structural and material parameters are listed in Fig. 2.)

skin depth at 40 GHz is about 0.4 μm, it is plausible to expect that the value of N_a should be closely related to the proper aspect ratio as reported in [11] and [12]. By having $N_1 = N_2 = N_4 = 160$, and $W/b = 0.1$, we set $N_a = 16$. Varying the value of N_m from 132 to 142, 144, 146, and 156, respectively, Fig. 3 plots the tangential electric field E_x at the $y = (h_1 + h_2 + t)^-$ and $y = (h_1 + h_2 + t)^+$ interfaces. The tangential fields just underneath the 5-μm-thick metal strip do not match well with those just above the metallized strip for $N_m = 132$ and 142. When $N_m = 146$ and 156, the interface field matchings seem to be good, but the nearly singular property imposed on the corner ($x = 0.45b$) of the good rectangular strip begins to degrade as the value of N_m is increased. Notice that the field matching properties can change substantially by subtracting or adding just two terms to $N_m = 144$. This is by no means a coincidence. It follows the rule of aspect ratio, i.e., $N_m = N_{31} + N_{33} = 160 \times (1 - 0.1) = 144$.

To give a broader idea on the effects of the relative convergence criterion for the particular case study, Fig. 4 plots the normalized propagation constant against the number of metal modes N_m using N_2 ($N_1 = N_2 = N_4$) as the controlling parameter. The data points under the circle (○) signs are for those obeying the relative convergence criterion confirmed earlier in Fig. 3. For each value of N_2, the normalized propagation constant may change drastically as N_m changes. The contour of the circle signs, however, represents a smooth convergence property against N_m and converges quickly, as shown in Fig. 4, for the normalized propagation constant.

Both the relative and absolute convergence studies depicted in Figs. 3 and 4 can be illustrated together as shown in Fig. 5, which plots the normalized propagation constant and conductor loss on both the left and right axes against the normalized gap width (W/b), respectively, using a different number of expansion terms N_2 ($N_1 = N_2 = N_4$) and N_m. The value of N_m is determined by the aspect ratio discussed in Fig. 3. When the finline has a narrow gap width, and consequently a smaller W/b ratio, our formulation requires that N_2 be over 80 for solutions with better convergence, as shown in Fig. 5. The fact that the conductor loss converges slower than that of the propagation constant is clear in these plots. Each conductor loss plot is distinguishable from others, whereas the plot for the propagation constant overlaps for N_2 greater than 120. Higher loss for the finline with smaller gap is understandable since the dominant mode electromagnetic field line is concentrated near the gap of the finline. This in turn will cause higher conductor loss associated with the metal fins.

V. The Combined Effects of Finite Conductivity and Thickness on a Lossy Finline

The power of the full-wave approach presented in this paper will be investigated by a case study, which investigates the same unilateral finline with the structural parameters given in Fig. 2. The test conditions for our formulation are shown in Fig. 6. Given an operating frequency of 40 GHz, the solid lines in Fig. 6 are the corresponding plots of the normalized propagation constant (β/β_0) and conductor loss with respect to the metallization thickness t. The conductor loss increases gradually as t is reduced from 10 to 0.01 μm. Here caution should be exercised. The absolute lower limit to the macroscopic domain imposed on the Maxwell equations with a continuous dielectric constant is 100 Å (10^{-2} μm) [16]. When t reaches a value of 10^{-6} μm, it is regarded as a *numerical* limiting case analysis of the present formulation for an *infinitely thin* conductor. If the

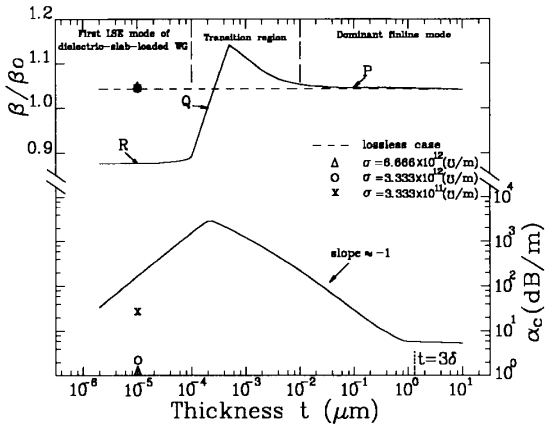

Fig. 6. Complex propagation constant of the dominant mode versus the metallization thickness t. $\sigma = 3.333 \times 10^7$ mhos/m, $W/b = 0.1$, and frequency = 40 GHz. (Other structural and material parameters are listed in Fig. 2.)

physical environment *were* to support the Maxwell equations in the limiting case analysis, we would not only test the validity of the present formulation but also establish the validity of using the assumption of an *infinitely thin perfect conductor* for analyzing lossless planar or quasi-planar structures [8], [9].

The skin depth obtained for the test case is 0.436 μm. As the value of t is reduced from 1 μm (2.3δ) to 0.01 μm (0.023δ), the excited currents start to distribute themselves throughout the entire cross section of the thin rectangular metal strip. The cross-sectional area also becomes smaller as t is reduced. Thus the ohmic loss increases. The slope for the conductor loss curve is nearly -1. This is a manifestation of the fact that the electromagnetic fields are uniformly distributed inside the rectangular strip and consequently the conductor loss is inversely proportional to the thickness t.

When t is reduced from 10^{-2} to 10^{-4} μm (1 Å), the conductor loss rises and declines. This is the region where a mode conversion takes place gradually. When the thickness t is reduced further from 10^{-4} to 10^{-6} μm, the conductor loss becomes smaller. This region corresponds to the familiar first LSE mode region; i.e., the finline essentially becomes a dielectric-slab-loaded waveguide. The field distribution is no longer that of a dominant finline mode, which carries most of the electromagnetic energy in the vicinity of the gap between the metal fins. Therefore the loss is smaller.

Next we test our formulation under the extreme condition that simulates the situation as an *infinitely thin perfect conductor*. This is done by increasing the conductivity by more than five orders of magnitude and reducing the thickness by five orders of magnitude from 1 μm. The results indicated by the triangle, circle, and cross signs show that the normalized propagation constant is very close to the solid line in the dominant mode region, and the conductor loss is decreased by increasing the conductivity from 3.333×10^{11} mhos/m to 6.666×10^{12} mhos/m. Increasing the conductivity by another five orders of magnitude, to 6.666×10^{17} mhos/m, the resulting dashed line represents the lossless case.

It is obvious, based on the analyses presented above, that care should be exercised in extracting design parameters such as the propagation constant from a full-wave field-theory analysis of a quasi-planar transmission line assuming *infinitely thin perfect conductor* strips. It is implied in Fig. 6 that the thickness t should be about three skin depths or more to have the smallest conductor loss and to have the propagation constant closer to the theoretical prediction when assuming *infinitely thin perfect conductors*.

The electric field patterns corresponding to the points P, Q, and R in Fig. 6 in the dominant finline mode, transition, and the first LSE mode regions are plotted in, respectively, parts (a), (b), and (c) of Fig. 7. It is easy to identify that parts (a) and (c) are for the dominant finline mode and the familiar first LSE mode of a dielectric-slab-loaded waveguide, respectively. On the other hand, part (b) gives no clear indication of which mode the field pattern represents. Therefore point Q belongs to the transition region.

VI. Other Theoretical Results

A comparison between the results obtained by this paper and the perturbational method [8], [9] is illustrated in Fig. 8. The results based on the perturbational method include the conductor losses of the waveguide housing and fins. In the limiting case where $W/b = 1$, i.e., a dielectric-slab-loaded WR-28 waveguide, the conductor loss given by the dashed line [8] seems to be more accurate. As W/b is reduced, the conductor loss in the broken line is close to the measured value [9]. Since our results in the solid line consider only the conductor losses of the metal fins, an accuracy comparison will be difficult. When the W/b ratio is less than 0.3, our results are approximately twice those obtained by [8]. As W/b approaches unity, the conductor loss in the solid line reduces to zero. This validates our solutions for conductor losses since the waveguide housing is assumed to be a perfect conductor in our analysis.

Fig. 9 plots the real parts of the characteristic impedance under the power–voltage definition [1], [12] and the normalized propagation constant against the normalized gap width. The data points with the circle signs are obtained by assuming lossless conductors. The imaginary parts of these curves are at least four orders of magnitude smaller and are not reported here. It is important to emphasize again that in practice a circuit designer should choose a good, thick metal coating for finline and other quasi-planar transmission lines if the actual physical design parameters are not to deviate from those obtained by assuming lossless conductors. Finally, Fig. 10 shows the effects of different conductivities on the conductor losses of the finline. As expected, lower conductivity will result in higher ac resistance for the metallization and consequently higher conductor losses for the finline.

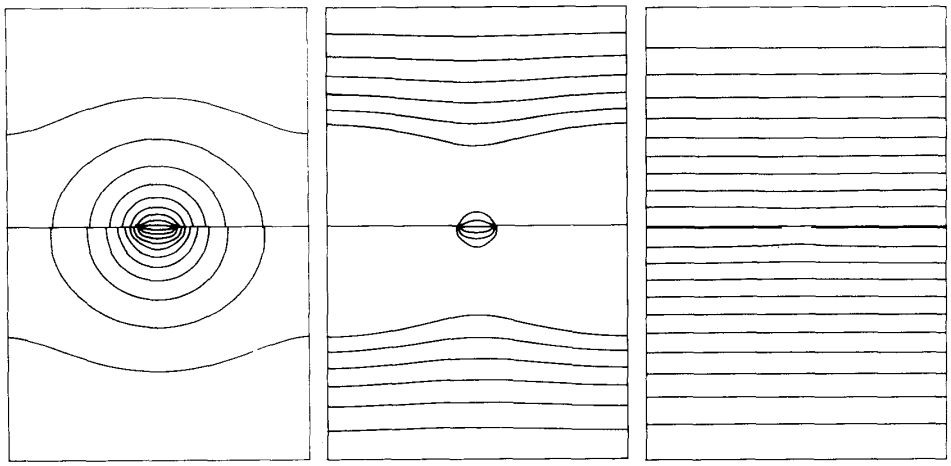

Fig. 7. Electric field patterns of the different modes at (a) point P, (b) point Q, (c) point R of Fig. 6. $\sigma = 3.333 \times 10^7$ mhos/m, $W/b = 0.1$, and frequency = 40 GHz. (Other structural and material parameters are listed in Fig. 2.)

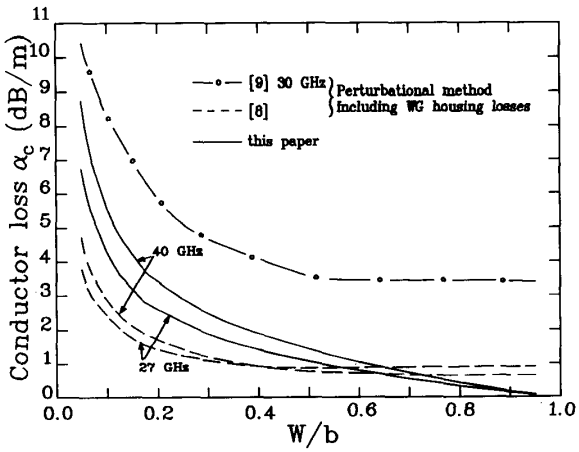

Fig. 8. Conductor loss α_c of the dominant mode versus the normalized fin gap W/b; $\sigma = 3.333 \times 10^7$ mhos/m and frequency = 40 GHz. (Other structural and material parameters are listed in Fig. 2.)

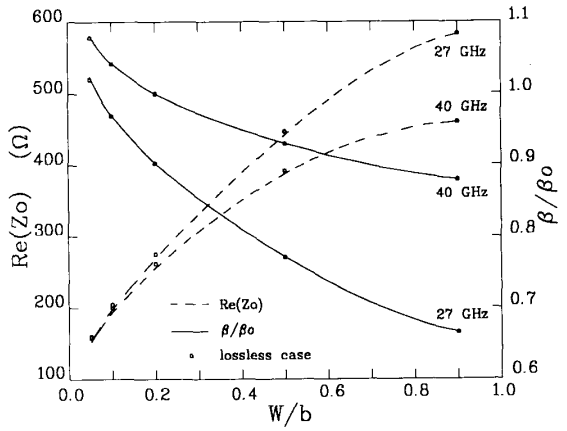

Fig. 9. Characteristic impedance $\mathrm{Re}(Z_0)$ and the normalized phase constant β/β_0 of the dominant mode versus the normalized fin gap W/b. $t = 5$ μm, and $\sigma = 3.333 \times 10^7$ mhos/m. (Other structural and material parameters are listed in Fig. 2.)

VII. Conclusion

Full-wave theoretical analyses of a gold-plated unilateral finline have been presented. The mode-matching full-wave approach incorporating the metal modes has proved to be very accurate and reliable for analyzing lossy millimeter-wave quasi-planar transmission lines. Without including the metal modes or satisfying the relative convergence criterion for the particular case study on a unilateral finline with good, thick (one order of magnitude greater than the skin depth) metal coating, the tangential electric field matchings become poor and result in inaccurate electromagnetic solutions.

A limiting case study for the particular finline, under the condition that the metallization thickness t of Fig. 2 approaches a value far below the limit of the Maxwell equations [16], shows that a mode conversion between the dominant finline mode and the first LSE dielectric-slab-loaded waveguide mode is *numerically* possible. The same limiting case study exposes two interesting aspects of the present full-wave formulation.

First, when the good conductor coating is of the order of a skin depth or less, the conductor loss is essentially ohmic with current flowing evenly inside the metal strip. Second, the commonly accepted assumption of an *infinitely thin perfect conductor* for use in many field theory analyses of millimeter-wave quasi-planar transmission lines is validated and proved to be a numerical limiting case of the present formulation.

It is also confirmed that the dispersion parameters of a *lossy* finline are in good agreement with those obtained by assuming *lossless* metallizations if the lossy finline is formed by a good, thick metal coating. In practice, a circuit designer should keep this in mind to reduce conductor loss and manage to use the dispersion parameters generated by a field theory package assuming infinitely thin perfect conductors.

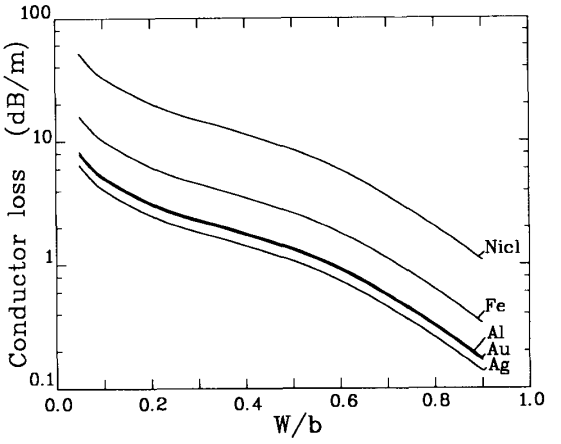

Fig. 10. Conductor loss of the dominant mode versus the normalized fin gap W/b under different controlling parameters. $\sigma_{Nicl} = 0.10 \times 10^7$ mhos/m, $\sigma_{Fe} = 1.03 \times 10^7$ mhos/m, $\sigma_{Al} = 3.82 \times 10^7$ mhos/m, $\sigma_{Au} = 4.10 \times 10^7$ mhos/m, $\sigma_{Ag} = 6.17 \times 10^7$ mhos/m. Frequency = 40 GHz, and $t = 5$ μm. (Other structural and material parameters are listed in Fig. 2.)

Acknowledgment

The authors would like to thank J.-T. Kuo, who verified the data shown in Fig. 1 by the SDA.

References

[1] T. Itoh, "Overview of quasi-planar transmission lines," *IEEE Trans. Microwave Theory Tech.*, vol. 37, pp. 275–280, Feb. 1989.

[2] Y. Fukuoka, Y.-C. Shih, and T. Itoh, "Analysis of slow-wave coplanar waveguide for monolithic integrated circuits," *IEEE Trans. Microwave Theory Tech.*, vol. MTT-31, pp. 567–573, July 1983.

[3] T.-C. Mu, H. Ogawa, and T. Itoh, "Characteristics of multiconductor, asymmetric, slow-wave microstrip transmission lines," *IEEE Trans. Microwave Theory Tech.*, vol. MTT-34, pp. 1471–1477, Dec. 1986.

[4] T. E. van Deventer, P. B. Katehi, and A. C. Cangellaris, "An integral equation method for the evaluation of conductor and dielectric losses in high-frequency interconnects," *IEEE Trans. Microwave Theory Tech.*, vol. 37, pp. 1964–1972, Dec. 1989.

[5] H.-Y. Lee and T. Itoh, "Phenomenological loss equivalence method for planar quasi-TEM transmission lines with a thin normal conductor or superconductor," *IEEE Trans. Microwave Theory Tech.*, vol. 37, pp. 1904–1909. Dec. 1989.

[6] W. Heinrich, "Full-wave analysis of conductor loss on MMIC transmission lines," in *1989 IEEE MTT-S Int. Microwave Dig.*, pp. 911–914.

[7] J.-T. Kuo and C.-K. C. Tzuang, "Complex modes in suspended coupled microstrip lines," *IEEE Trans. Microwave Theory Tech.*, vol. 38, pp. 1278–1286, Sept. 1990.

[8] D. Mirshekar-Syahkal and J. Brian Davies, "An accurate, unified solution to various fin-line structures, of phase constant, characteristic impedance, and attenuation," *IEEE Trans. Microwave Theory Tech.*, vol. MTT-30, pp. 1854–1861, Nov. 1982.

[9] C. A. Olley and T. Rozzi, "Characterisation of unilateral finline mode spectrum including loss analysis," in *Proc. 16th European Microwave Conf.*, 1986, pp. 511–516.

[10] T. S. Chu, T. Itoh, and Y.-C. Shih, "Comparative study of mode-matching formulations for microstrip discontinuity problems," *IEEE Trans. Microwave Theory Tech.*, vol. MTT-33, pp. 1018–1023, Oct. 1985.

[11] F. Alessandri, U. Goebel, F. Melai, and R. Sorrentino, "Theoretical and experimental characterization of nonsymmetrically shielded coplanar waveguides for millimeter-wave circuits," *IEEE Trans. Microwave Theory Tech.*, vol. 37, pp. 2020–2027, Dec. 1989.

[12] W.-K. Wang, C.-K. C. Tzuang, J.-S. Chang, and T.-H. Wang, "Investigations of complex modes in a generalized bilateral finline with mounting grooves and finite conductor thickness," *IEEE Trans. Microwave Theory Tech.*, vol. 37, pp. 1891–1897, Dec. 1989.

[13] T. Itoh, Ed., *Numerical Techniques for Microwave and Millimeter-Wave Passive Structures*. New York: Wiley, 1989, chs. 1 and 9.

[14] S. T. Peng, C.-K. C. Tzuang, and C.-D. Chen, "Full-wave analysis of lossy transmission lines incorporating the metal modes," in *1990 IEEE MTT-S Int. Microwave Symp. Dig.*, pp. 171–174.

[15] R. E. Collin, *Field Theory of Guided Waves*. New York: McGraw-Hill, 1960, chs. 5 and 6.

[16] J. D. Jackson, *Classical Electrodynamics*, 2nd ed. New York: Wiley, 1975, pp. 226–228.

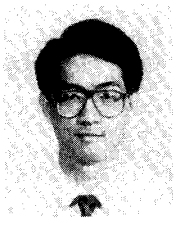

Ching-Kuang C. Tzuang (S'84–M'86) was born in Taiwan on May 10, 1955. He received the B.S. degree in electronic engineering from the National Chiao Tung University, Hsinchu, Taiwan, in 1977 and the M.S. degree from the University of California at Los Angeles in 1980.

From February 1981 to June 1984, he was with TRW, Redondo Beach, CA, working on analog and digital monolithic microwave integrated circuits. He received the Ph.D. degree in electrical engineering in 1986 from the University of Texas at Austin, where he worked on high-speed transient analyses of monolithic microwave integrated circuits. Since September 1986, he has been with the Institute of Communication Engineering, National Chiao Tung University, Hsinchu, Taiwan, R.O.C. His research activities involve the design and development of millimeter-wave and microwave active and passive circuits and the field theory analysis and design of various quasi-planar integrated circuits.

Chu-Dong Chen (S'89) was born in Taiwan on March 14, 1956. He received the B.S. degree in electronic engineering from Chung Yuan University in 1978 and the M.S. degree in electronic engineering from the National Chiao Tung University, Hsinchu, Taiwan, in 1980.

From 1981 to 1988, he was with the Chung Shan Institute of Science and Technology, Lung Tan, Taiwan, as an assistant researcher. He had been involved in the design and development of millimeter-wave and microwave III–V compound semiconductor devices. Since 1988, he has been pursuing the Ph.D. degree at the National Chiao Tung University. His current research interests include the rigorous field analysis of quasi-planar transmission lines and the design of millimeter-wave components.

Song-Tsuen Peng (M'74–SM'82–F'88) was born in Taiwan, Republic of China, on February 19, 1937. He received the B.S. degree in electrical engineering from the National Cheng-Kung University in 1959 and the M.S. degree in electronics from the National Chiao-Tung University in 1961, both in Taiwan, and the Ph.D. degree in electrophysics from the Polytechnic Institute of Brooklyn, Brooklyn, NY, in 1968.

From 1968 to 1983, he held various research positions with the Polytechnic Institute of Brooklyn. Since 1983, he has been a Professor of Electrical Engineering and Director of the Electromagnetics Laboratory at the New York Institute of Technology, Old Westbury, NY. He has been active in the fields of wave propagation, radiation, diffraction, and nonlinear electromagnetics and has published numerous papers on electromagnetics, optics, and acoustics.

Dr. Peng is a member of Sigma Xi.